European Journal of Molecular & Clinical Medicine
ISSN 2515-8260 Volume 07, Issue 9, 2020

An Efficient Zernike Moments with Logistic Regression Classifier based Skin Lesion Diagnosis using Dermoscopic Images

[1]R.Thanga Selvi, [2]A. Ramalingam
[1]Assistant Professor, Department of Computer Science and Engineering, Vel Tech Rangarajan Dr Sagunthala Rangarajan R&D Institute of Science and Technology, Chennai.
[2]Professor, Department of Master of Computer Applications, Sri Manakula Vinayagar Engineering College. Puducherry.
Email: golda.selvi@gmail.com, a.ramalingam1972@gmail.com

Abstract

Diagnosis of skin cancer acts as a vital part of the early and accurate detection of skin lesions using dermoscopic imaging. However, the automatic skin lesion diagnosis becomes hard owing to the existence of artifacts, indistinct boundary, poor contrast, and distinct size and shape of the lesion. This study introduces a novel Zernike Moments (ZM) with Logistic Regression Classifier (LRC), named ZM-LRC model for skin lesion diagnosis using dermoscopic images. The presented ZM-LRC model comprises four stages namely pre-processing, segmentation, feature extraction, and classification. The ZM-LRC model performs image segmentation using Shannon's Entropy with Brainstorm optimization (BSO) algorithm. Besides, the ZM based feature extraction and LRC oriented classification processes are carried out. Elaborative experimental analysis was carried out on ISIC dataset and the obtained results are investigated with respect to distinct performance measures. The attained simultaion values signified the effective diagnostic outcome of the ZM-LRC model with a higher sensitivity of 95.78%, specificity of 97.86%, and accuracy of 98.56%.

Keywords: Skin lesions, Dermoscopy, ISIC dataset, Zernike moment, Logistic regression

1. Introduction

Melanoma is an inoperable class of skin cancers where the existence rate has been improved in last decades. Based on the survey provided by World Health Organization (WHO), maximum number of users have reported skin lesions. Moreover, [1] addressed that prediction of melanoma in earlier stages results in increasing the lifespan of an individual. Dermatoscopy is defined as non-invasive medical application applied for melanoma prediction which is performed by applying the gel on defected skin and starts to examine by a dermoscope. It examines the sub surface architecture of defected skin which is not seen by human eye. Using the clinical strategy, skin lesion is amplified several times and makes the prediction into simple process. In order to diagnose melanoma, dermatologists depend upon ABCD principle, 7 point checklist, and Menzie model. Though the above-defined approaches of manual examination have exhibited better performance, it is still challenging due to the factors called a huge number of patients, manual error, infrastructure, and so on. Moreover, physician diagnosis might be subjective, as it depends on the medical experience and human vision.

In order to overcome these limitations, the automatic system has to be employed to discriminate benign and melanoma at earlier levels. Computer aided diagnosis (CAD) is beneficial to doctors by applying technical deployments in dermoscopy and offers an additional suggestion. The CAD models apply different Machine Learning (ML) models, for instance, extraction of different features like colors, shapes, and textures from a dermoscopic picture and using classifiers. The classifier methods are dependent on extracted features for training, which are classified as 3 major phases namely, Low, Mid, and Higher levels. Different types of previous

approaches make use of features gained from combination of feature vectors. The feature fusion model enhances the classification accuracy by considering the benefits of host schemes, however, the processing time and storage demands are enhanced.

Various CAD models [2] were presented for melanoma prediction and attempts to reflect the process computed by dermatologists which depend upon the rank of features extracted under the application of ML technologies. Usually, these systems are operated on 4 basic steps namely, pre-processing, lesion segmentation, feature extraction, and selection, as well as classification. Segmentation of skin lesions are referred to be the basic steps with have long-lasting impacts on classification tasks. Accurate lesion segmentation is said to be arduous process because of many reasons like grade of lesion size, shape, color, and texture. Followed by, a smooth changeover occurs between skin color and lesion. Moreover, some other limitations are specular refection, existence of hair, inclination toward the edge, air, and fluid bubble.

[3] presented a model to eliminate undesirable hair from lesions before segmentation process. Subsequently, feature extraction is carried out with the help of color as well as texture features. To classify data, Support Vector Machine (SVM), and K-nearest neighbor (KNN) have been employed. Likewise, [4] employed a hybridization approach to segment hair by the combination of convolution as well as recurrent layers. Here, it has applied deep encoded features for hair inclination, that has been projected to recurrent layers for scratching the spatial dependencies over incoherent images. [5] employed robust marching and 2D derivation of Gaussian inpainting mechanism for hair noise elimination. [6] utilized automated model for segmentation. Here, otsu's thresholding has been applied for segmentation, and texture feature extraction of Local Binary Pattern (LBP) has been employed. The Neural Network (NN) classification models are applied for classification and validated by means of sensitivity and specificity.

[7] introduced the optimized clustering evaluation by applying neutrosophic graph cut (OCE-NGC) approach to compute segmentation. Bio-inspired framework (genetic algorithm (GA)) has been utilized for optimizing the histogram-relied clustering strategy, which explores the best centroid values. Besides, the pixels are collected with the help of defined threshold values by applying neutrosophic c means approach. Consequently, a graph-cut model [8] is executed to segment the forefront and backdrop portion of dermoscopic photographs. [9] presented a saliency on the basis of segmentation approach where the prediction of background depends upon the spatial layout like color and boundary details. In order to reduce the prediction error, Bayesian approach has been applied. Features are important in classification process and extracted by local, global scenarios.

[10] applied a local-global approach to predict melanoma from dermoscopic images. Local schemes have been considered for extracting the features under the application of bag-of-words (BoW), whereas global approaches are identified for skin lesions classification. Challenging results have been accomplished by means of maximum sensitivity and specificity. [11] recommended a perceptually based approach for border prediction and combine the efficiency of edge as well as region based segmentation. Followed by, hill-climbing schemes are used to determine the region of interest (ROI), and adaptive threshold approach for predicting best lesion border. [12] projected cross-correlation based models for feature extraction and perform skin lesion classification. Kernel patches are used according to the type of skin disease which is categorized by using multi-label ensemble multi-class classifier.

This study introduces a novel Zernike Moments (ZM) with Logistic Regression Classifier (LRC), named ZM-LRC model for skin lesion diagnosis using dermoscopic images. The presented ZM-LRC model encompasses four stages like pre-processing, segmentation, feature extraction, and classification. The ZM-LRC model accomplishes image segmentation using Shannon's Entropy (SE) with Brainstorm optimization (BSO) algorithm. In addition, the ZM based feature extraction and LRC based classification processes are carried out. A comprehensive set of investigations were performed using ISIC dataset and the attained results are examined with respect to distinct evaluation metrics.

2. The Proposed ZM-LRC Model

The workflow of the presented ZM-LRC model is displayed in Fig. 1. The figure implied that the dermoscopic images from the ISIC dataset are initially preprocessed by the use of GK filtering. Followed by, the SE-BSO algorithm is applied to determine the infection of lesion regions in the region. Next, the ZM technique is executed to extract feature vectors from the segmented image. Lastly, the feature vectors are fed into the LRC model to allocate the appropriate class labels.

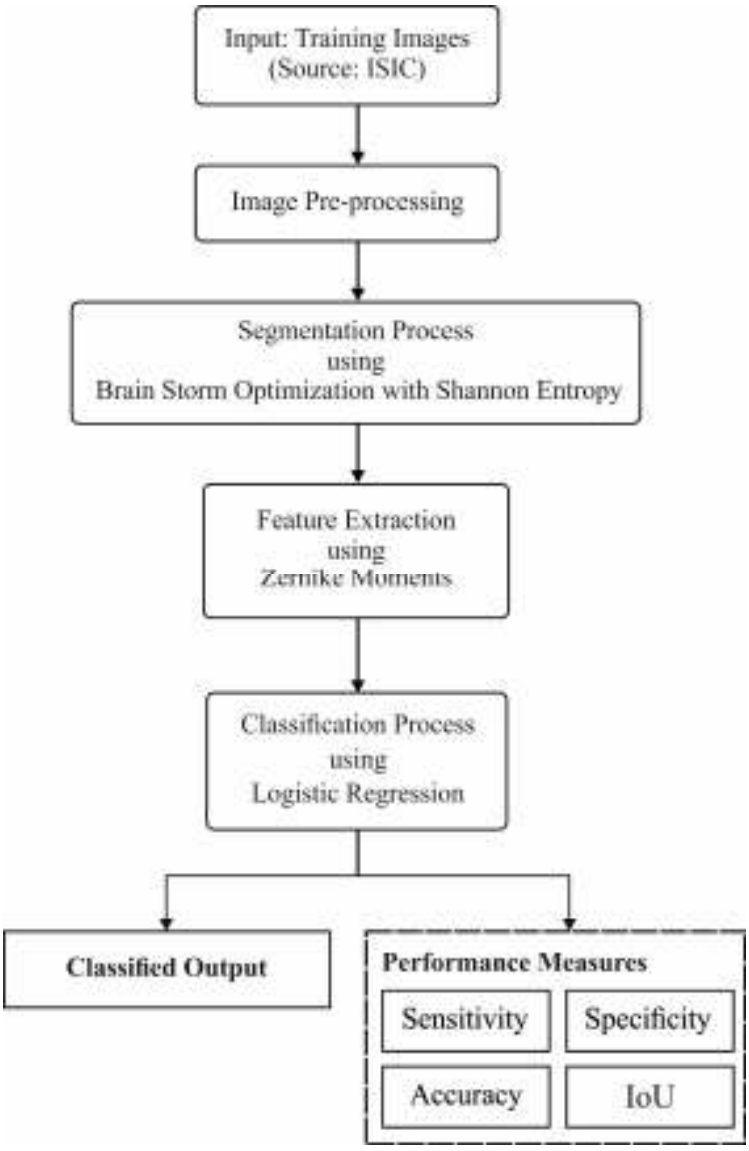

Fig. 1. Overall Process of Proposed ZM-LRC Method

2.1. Image Pre-processing

Gabor Kuwahara filter is deployed using Gabor transformation and remarkable Kuwahara filter. The paradigm of Gabor Kuwahara filter is applied for melanoma prediction. It is composed of 2 stages. Firstly, an input image is transformed using Gabor transformation.

2.2. Image Segmentation using BSO based Shannon's function

If the input image is pre-processed, then segmentation is carried out with the help of BSO-SE. It is contributed to SE reliant segmentation as well as best threshold values are selected by BSO.

2.2.1. Shannon's Function

Actually, entropy is used for estimating the uncertainties of an image. Initially, decide an image frame size $M * N$. Then, a gray value of pixel with coordinates (a, b) are represented as $f\ (a, b)$, for $a\ \in \{1, 2, \ldots, M\}$ and $b\ \in \{1, 2, \ldots, N\}$. Consider that L is a gray level image I_0 and set of gray levels $\{0,1,2, \ldots, L-1\}$ are implied as G where:

$$f(a, b) \in G \forall (a, b) \in image \tag{1}$$

The normalized histogram of an image is illustrated as $H = \{h_0, h_1, \ldots, h_{L-1}\}$. For multi-thresholding problem, the given function is demonstrated as;

$$H(T) = h_0(t_1) + h_1(t_2), \ldots, h_{L-1}(t_{k-1}) \tag{2}$$

$$T * \max_{T}\{H(T)\} \tag{3}$$

where T^* implies the best threshold value that is decided using BSO.

2.2.2. BSO algorithm

The brainstorming mechanism is applied extensively for several issues which are resolved by a single user. The major theme of brainstorming is to produce diverse opinions and best solutions are accomplished to resolve certain issues from the extracted ideas.

In general, BSO is defined as a novel population-reliant Swarm Intelligence (SI) model evolved by human brainstorming task. The BSO emanates n arbitrary feasible solutions and estimates them on the basis of Fitness Function (FF). Based on the [13], BSO is composed of 3 phases namely, clustering individuals, interruption of cluster center, and developing solution. The BSO collects n individuals as m clusters with the help of k means clustering method. Thus, identical solutions are grouped jointly in all generations. Hence, a novel solution is produced with possibility of P, and it substitutes a cluster center, by the cluster center interruption. Consequently, BSO emanates an individual with the help of single cluster or combination of clusters. Besides, BSO selects an individual according to the cluster(s) center(s), as follows:

$$X_{selecfed=} \begin{cases} X_i, & one\ \ cluster \\ rand\ \times X_{1i} + (1 - rand) \times X_{2i}, & two\ clusters \end{cases} \tag{4}$$

where X_{1i} and X_{2i} defines the ith dimension of decided clusters, and *rand* implies the arbitrary value from 0 and 1. BSO upgrades the decided individual in the following:

$$X_{new} = X_{selected} + \xi * random(0,1) \tag{5}$$

where arbitrary is defined as a Gaussian arbitrary value with 0 mean as well as unit variance, correspondingly; ξ indicates the modifying factor,

$$\xi = logsin\left(\frac{0.5 * m_i - c_i}{k}\right) \text{x rand} \tag{6}$$

Where m_i and c_i denotes the higher count of iterations as well as present iteration; *logsin*() refers the logarithmic sigmoid function, *rand*() represents the random measure among 0 and 1, and k signifies the changing value for slope of *logsin*() function.

2.3. Feature Extraction

To extract the feature vector from the segmented skin lesion image, ZM is applied. The ZMs [14] are defined as orthogonal moment attained by presenting the input images as complicated orthogonal Zernike polynomial (basis function). The ZM of order p as well as repetition q for the function $f(x, y)$ across a unit disk described by,

$$Z_{pq} = \frac{p+1}{\pi} \int \int_{x^2+y^2 \leq 1} f\,(x,y) V_{pq}^{*}(x,y) dxdy \tag{7}$$

Where p implies the non-negative integer, q denotes the integer in which $0 \leq |q| \leq p$, and $p - |q| = even$. The function $V_{pq}^{*}(x, y)$ is a complex conjugate of Zernike orthogonal basis function $V_{\mathrm{pq}}(x, y)$ that is illustrated as:

$$V_{\mathrm{pq}}(x,y) = V_{\mathrm{pq}}(r,\theta) = R_{\mathrm{pq}}(r) \exp(\mathrm{jq}\theta) \tag{8}$$

where $= \sqrt{x^2 + y^2}$, $\theta = \tan^{-1}\left(\frac{y}{\chi}\right)$, $0 \leq \theta \leq 2\pi, j = \sqrt{-1}$. The radial polynomial $R_{pq}(r)$ is demonstrated as:

$$R_{pq}(r) = \sum_{s=0}^{(p-|\mathrm{q}|)/2} (-1)^s \frac{(p-s)!}{s!\left(\frac{p+|\mathrm{q}|}{2}-s\right)!\left(\frac{p-|\mathrm{q}|}{2}-s\right)!} (r)^{p-2s} \tag{9}$$

The zeroth-order approximation of Eq. (7) is provided

$$Z_{pq} = \frac{2(p+1)}{\pi N^2} \sum_{i=0}^{N-1} \sum_{\mathrm{k}=0}^{N-1} f\,(x_i, y_k) R_{pq}(r_{ik}) e^{-j\mathrm{q}\theta_{ik}} \tag{10}$$

Where (x_i, y_k)denotes the generalized coordinate position which corresponds to pixel (i, k) gained by using the coordinate conversion:

$\chi_i = \frac{2i+1-N}{N\sqrt{2}}, y_k = \frac{2k+1-N}{N\sqrt{2}},$

for all i, $\mathrm{k} = 0, 1, 2, \ldots N-1$. The outer unit disk for ZMs processing is performed to show considerable performance for ZMs-based image pattern matching issues. Additionally, in presented ZMs-reliant framework, there is no requirement of moments with false q, since $|Z_{p,q}| = |Z_{p,-q}|$.

2.4. Image Classification

Finally, LR is applied as a classification model to identify the exact class label of the input skin lesion image. In LR, the possibility of examining consequent variables comes under the appropriate class. At this point, the viability of inclusion is determined. Moreover, the application of LR enables to estimate the resolution of imaging application. Assume the data set in executing the response parameter which comes under the binary file. For every finite component the training data $D = \{\{a_i, b_i\}\}_{1 \le i \le n}$ has been evaluated in which $\{a_i\}_{1 \le i \le n}$ defines the sequence of input parameters, $\{b_i\}_{1 \le i \le n}$ means the vector of response variable, and $a_i \in R^m, b_i \in \{0,1\}$ for $1 \le j \le n$ and m count of value accomplished from transducers and sensors. When the finite component shows the inclusion, at that time, it is considered that $b_i = 1$; else, it is assumed as $b_i = 0$. Then, training set can be represented by $D = \{B, A\}$, where

$$B = \begin{bmatrix} b_1 \\ b_2 \\ \vdots \\ b_n \end{bmatrix}, X = \begin{bmatrix} a_{11} & a_{12} & \cdots & a_{1m} \\ a_{21} & a_{22} & \cdots & a_{2m} \\ \vdots & \vdots & \vdots & \vdots \\ a_{n1} & a_{n2} & \cdots & a_{nm} \end{bmatrix} = \begin{bmatrix} a_{[1]} \\ a_{[2]} \\ \vdots \\ a_{[n]} \end{bmatrix}$$

Prediction of signal $a_i \in R^m$ acquired from sensors, then it is obligatory for classifying the existence of finite elements. The main aim of this method is to find a classifier $f: R^m \to \{0,1\}$, which enables classification of object as categories $b = 1$ or $b = 0$ according to the observation $a \in R^m$.

A random variable B is defined with binomial distribution, i.e., $B : \Omega \to \{0,1\}$ on probability space (Ω, F, P). LR is model where they B response variable is composed of binomial distribution. According to the input parameters A the LR [15] defines possibility of analysis of reliant variable B. Hence, it is essential to compute possibilities of success $(B = 1|A)$, and reduce $P(B = 0|A)$. Here, the odds are represented as given in Eq. (11):

$$\Theta(A) = \frac{P(B = 1|A)}{P(B = 0|A)} = \frac{P(B = 1|A)}{1 - P(B = 1|A)} \tag{11}$$

Therefore, odds are defined as ratio of probability of success to probability of defeat. LR is mainly applied to compute the possibility of success $p(A) = P(B = 1|A)$ which depends upon the observation A. As the possibility of success $p(A) \in (0,1)$, which depends upon Eq. (11) it provides the odds $\Theta(A) \in (0, \infty)$; however $ln(\Theta(A)) \in (-\infty, \infty)$. The logarithm of odds is meant to be log-odds or logit. In LR, linear dependencies from log-odds and input parameters are examined in Eq. (12):

$$ln\Theta(A) = ln\left(\frac{p(\beta, A)}{1 - p(\beta, A)}\right) = A\beta \tag{12}$$

where $\beta = (\beta_1, \ldots, \beta_m) \in R^m$. In linear Eq. (12) an intercept and the column corresponds to intercept in a matrix X. From Eq. (12), Eq. (13) is derived:

$$p(\beta, X) = \frac{e^{X\beta}}{1 - e^{X\beta}} \tag{13}$$

In general, to evaluate the unseen variable of β in Eq. (13), maximum likelihood method has been employed. Thus, a process showcased in Eq. (14) has to be resolved in which likelihood function

$$\max_{\beta} L(\beta, B, A) \tag{14}$$

is depicted as given in Eq. (15):

$$L\ (\beta, B, A) = \prod_{i=1}^{n} p\ (\beta, a_{(i)})^{b_i} (1\text{-}\, p(\beta, a_{(i)}))^{1-b_i} \tag{15}$$

The replacement to resolve Eq. (14), the auxiliary process is implied in Eq. (16):

$$\max_{\beta} l\ (\beta, B, A) \tag{16}$$

Where the objective function is described as logarithm of a likelihood function $l\ (\beta, B, A) = ln(L(\beta, B, A))$ and it reflects Eq. (17):

$$l\ (\beta, B, A) = \sum_{i=1}^{n} \left(b_i a_{(i)} \beta\ - \ln\left(1\ +\ e^{a_{(i)}\beta}\right)\right) \tag{17}$$

The Newton–Raphson mechanism is employed for estimating the unseen variables β. Submission of this method reasons that unknown parameters β are calculated in various iterations. Here, $j\ +\ 1$ the estimators are measured by Eq. (18):

$$\beta j + 1 = \beta j + \frac{\partial^2 l}{\partial \beta \partial \beta^{\mathrm{T}}} (\beta j)^{-1}\ \frac{\partial l}{\partial \beta} (\beta j) \tag{18}$$

where $\frac{\partial l}{\partial \beta} (\beta)$, $\frac{\partial^2 l}{\partial \beta \partial \beta^{\mathrm{T}}}$ (β) implies 1st and 2nd partial derivatives of objective function (17).

3. Experimental Validation

This section investigates the diagnostic results of the presented ZM-LRC model against the benchmark ISIC dataset [16]. It contains different classes of dermoscpic images. The results are assessed interms of different performance measures such as sensitivity, specificity, and accuracy. The details relevant to the dataset are given in Table 1 and few sample test images are illustrated in Fig. 2.

Table 1 Dataset Description

S. No	Classes	Number of Images
1	Angioma	21
2	Nevus	46
3	Lentigo NOS	41
4	Solar Lentigo	68

5	Melanoma	51
6	Seborrheic Keratosis	54
7	Basal Cell Carcinoma	37

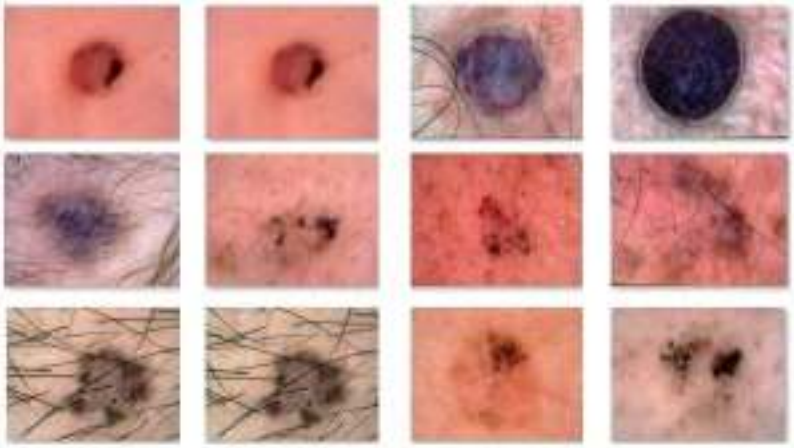

Fig. 2. Sample Skin Lesion Images

Fig. 3 illustrates the visualization results analysis of the projected technique on the applied dermoscopic images. Fig. 3a shows the input original image, and Figs. 3b-d showcases the preprocessed, masked, and segmented versions of the input image.

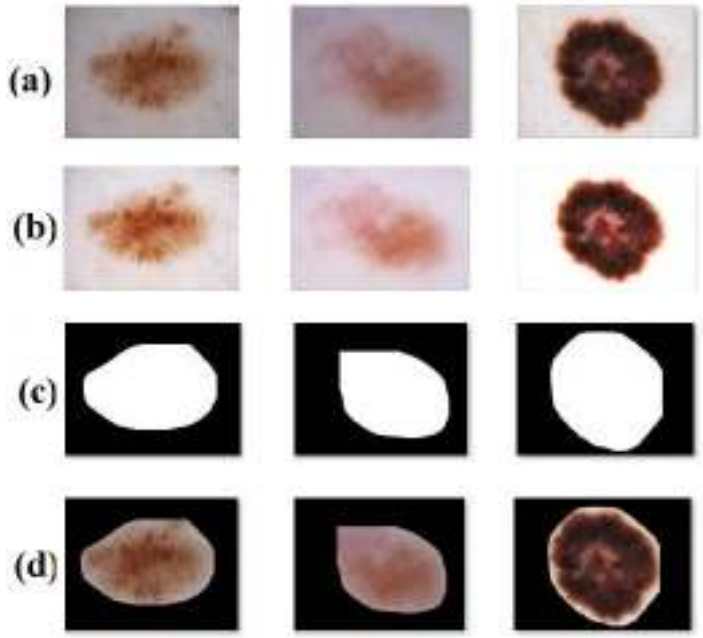

Fig. 3. a) Original Image b) Preprocessed Image c) Masked Image d) Segmented Image

Figs. 4-5 illustrates the comparative analysis of the presented ZM-LRC model with existing methods with respect to sensitivity, specificity, accuracy, and intersection of union (IoU). By

examining the diagnostic outcome interms of sensitivity, the methods devised by Li et al. and Yuan et al. have depicted inferior performance with the minimal sensitivity values of 82% and 82.5% respectively. At the same time, the method presented by AI-Masni et al. has offered a slightly higher sensitivity of 85.4%. Concurrently, the ResNet 50 and the method developed by Halil et al. have resulted in an even better sensitivity of 90% and 90.82%. Along with that, the VGG-19 SVM and Bi et al. models have demonstrated moderate outcomes with the sensitivity of 93% and 93.4% respectively. Simultaneously, the VGG-19 model has demonstrated competitive sensitivity of 95%. But the presented ZM-LRC model has accomplished effective outcomes by attaining a maximum sensitivity of 95.78%. By observing the diagnostic result interms of specificity, the ResNet-50 and VGG-19 models have demonstrated inferior performance with the least specificity values of 61% and 68% respectively. Simultaneously, the VGG-19 SVM model has offered a somewhat higher specificity of 69%. In line with this, the method developed by Bi et al. and Halil et al. has resulted in an even better specificity of 80.2% and 92.68%. Along with that, the method presented by AI-Mansni et al. and Yuvan et al. has exhibited moderate outcomes with the specificity of 96.69% and 97.5% correspondingly. Simultaneously, the method devised by Li et al. has demonstrated competitive specificity of 97.8%. However, the presented ZM-LRC model has accomplished an effective outcome by reaching the highest specificity of 97.86%.

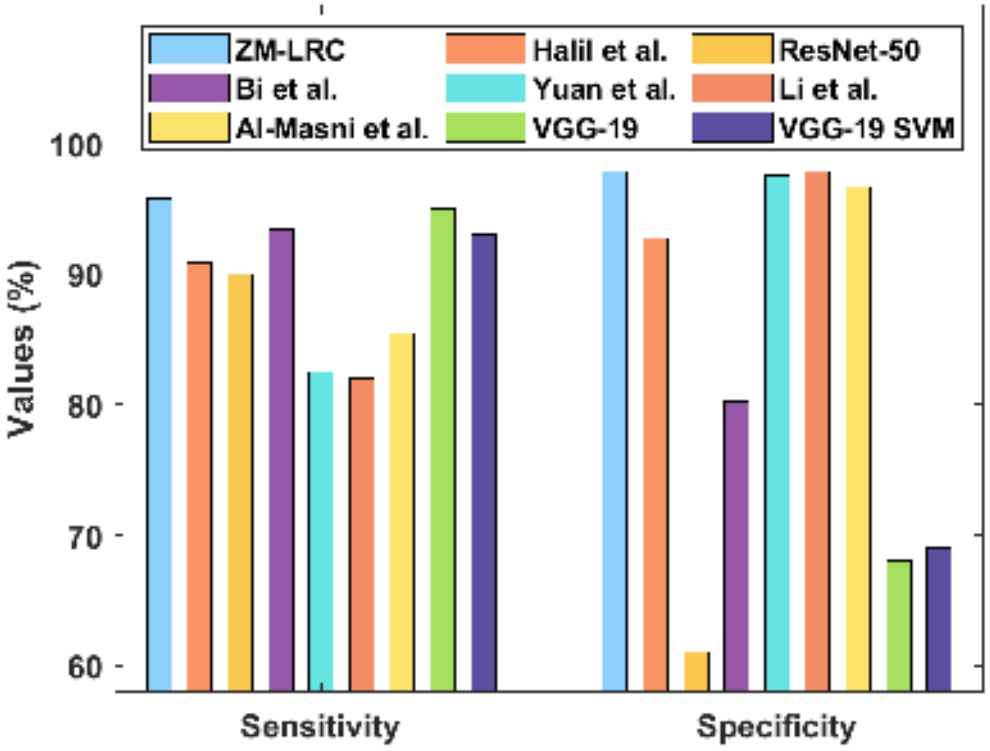

Fig. 4. Sensitivity and specificity analysis of ZM-LRC model

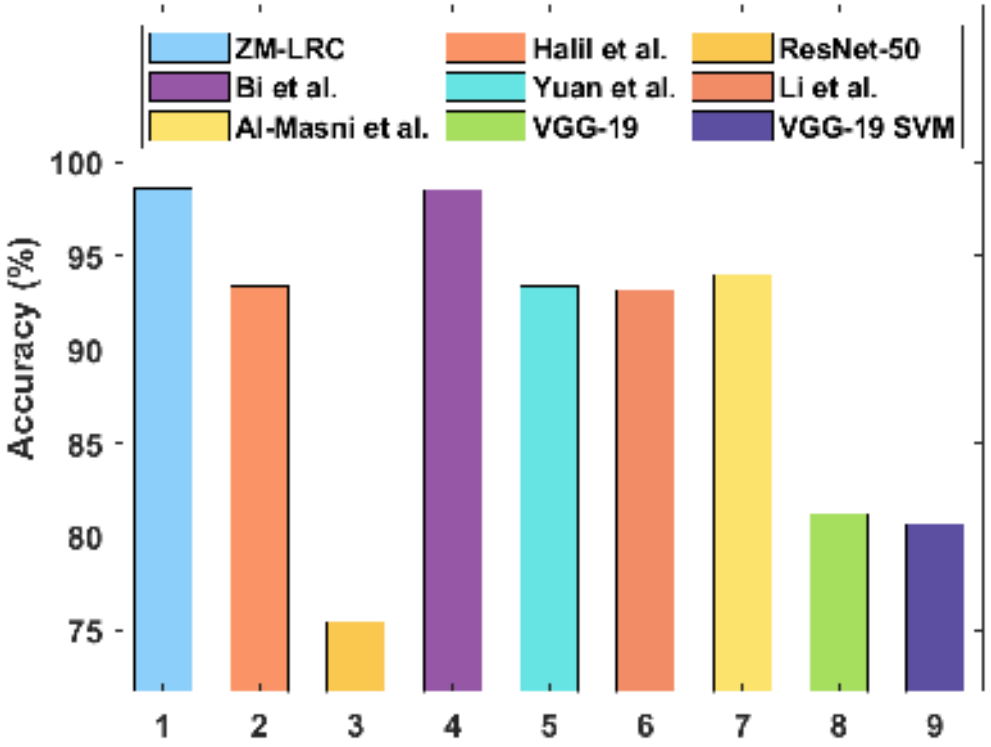

Fig. 5. Accuracy analysis of ZM-LRC model with existing methods

By examining the diagnostic outcome with respect to accuracy, the ResNet-50 and VGG-19 SVM models have depicted inferior performance with minimal accuracy values of 75.5% and 80.7% respectively. Likewise, the VGG-19 has offered a slightly higher accuracy of 81.2%. Similarly, the method developed by Li et al. and Halil et al. has resulted in even better accuracy of 93.2% and 93.39%. In line with, the methods devised by Yuvan et al. and AI-Masni et al. models have showcased moderate results with the accuracy of 93.4% and 94.03% correspondingly. Simultaneously, the method presented by Bi et al. has demonstrated competitive accuracy of 98.5%. But, the presented ZM-LRC model has accomplished effective outcomes by achieved a maximum accuracy of 98.59%. By investigative the diagnostic outcome with respect to IoU, the methods devised by Li et al. have exhibited inferior performance with the least IoU value of 86%. However, the proposed ZM-LRC model has accomplished effective results by obtaining the highest IoU of 88.5%.

4. Conclusion

This study has developed a novel ZM-LRC model for skin lesion diagnosis using dermoscopic images. The presented ZM-LRC model comprises four stages such as preprocessing, segmentation, feature extraction, and classification. Primarily, the dermoscopic images from the ISIC dataset are initially preprocessed by the use of GK filtering. Followed by, the SE-BSO algorithm is applied to determine the infection of lesion regions in the region. Next, the ZM technique is executed to extract feature vectors from the segmented image. Lastly, the feature vectors are fed into the LRC model to allocate the appropriate class labels. A comprehensive set of investigations were performed using ISIC dataset and the attained results are examined with respect to distinct performance measures. The attained experimental values signified the effective diagnostic outcome of the ZM-LRC model with a higher sensitivity of 95.78%, specificity of 97.86%, and accuracy of 98.56%. In future, the advanced deep learning architectures can be utilized in place of ZM technique.

References

[1] Barata C, Ruela M, Francisco M, Mendonca T, Marques J (2014) Two systems for the detection of melanomas in dermoscopy images using texture and color features. Syst J 8:965–979

[2] Marques JS, Barata C, Mendonca T (2012) On the role of texture and color in the classifcation of dermoscopy images. In: Annual international conference of the IEEE engineering in medicine and biology society (EMBC)

[3] Sumithra R, Suhil M, Guru DS (2015) Segmentation and classifcation of skin lesions for disease diagnosis. Procedia Comput Sci 45:76–85

[4] Attia M, Hossny M, Zhou H, Nahavandi S, Asadi H, Yazdabadi A (2019) Digital hair segmentation using hybrid convolutional and recurrent neural networks architecture. Comput Methods Progr Biomed 177:17–30

[5] Joseph S, Panicker JR (2016) Skin lesion analysis system for melanoma detection with an efective hair segmentation method. In: International conference on information science (ICIS). IEEE, New York, pp 91–96

[6] Cheerla N, Frazier D (2014) Automatic melanoma detection using multi-stage neural networks. Int J Innov Res Sci Eng Technol 3(2):9164–9183

[7] Hawas AR, Guo Y, Du C, Polat K, Ashour AS (2020) OCE-NGC: a neutrosophic graph cut algorithm using optimized clustering estimation algorithm for dermoscopic skin lesion segmentation. Appl Soft Comput 86:105931

[8] Hajiaghayi M, Kortsarz G, MacDavid R, Purohit M, Sarpatwar K (2020) Approximation algorithms for connected maximum cut and related problems. Theor Comput Sci 814:74–85

[9] Ahn E, Bi L, Jung YH, Kim J, Li C, Fulham M, Feng DD (2015) Automated saliency-based lesion segmentation in dermoscopic images. In: 2015 37th annual international conference of the IEEE engineering in medicine and biology society (EMBC). IEEE, New York, pp 3009-3012

[10] Barata C, Ruela M, Francisco M, Mendona T, Marques JS (2014) Two systems for the detection of melanomas in dermoscopy images using texture and color features. IEEE Syst J 8(3):965–979

[11] Qaisar A, Garcia IF, Emre Celebi M, Ahmad W, Mushtaq Q (2013) A perceptually oriented method for contrast enhancement and segmentation of dermoscopy images. Skin Res Technol 19(1):e490–e497

[12] Chatterjee S, Dey D, Munshi S, Gorai S (2019) Extraction of features from cross correlation in space and frequency domains for classifcation of skin lesions. Biomed Signal Process Control 53:101581

[13] Pourpanah, F., Shi, Y., Lim, C.P., Hao, Q. and Tan, C.J., 2019. Feature selection based on brain storm optimization for data classification. *Applied Soft Computing*, *80*, pp.761-775.

[14] Kumar, Y., Aggarwal, A., Tiwari, S. and Singh, K., 2018. An efficient and robust approach for biomedical image retrieval using Zernike moments. *Biomedical Signal Processing and Control*, *39*, pp.459-473.

[15] Rymarczyk, T., Kozłowski, E., Kłosowski, G. and Niderla, K., 2019. Logistic Regression for Machine Learning in Process Tomography. *Sensors*, *19*(15), p.3400.

[16] https://isic-archive.com/